Dyes and Pigments 92 (2012) 1337–1343

Contents lists available at SciVerse ScienceDirect

Dyes and Pigments

journal homepage: www.elsevier.com/locate/dyepig

A novel rhodamine-based fluorescent and colorimetric "off–on" chemosensor and investigation of the recognizing behavior towards Fe^{3+}

Mengyao She [a], Zheng Yang [a], Bing Yin [a,c], Jin Zhang [a], Jia Gu [a], Wenting Yin [a], Jianli Li [a,*], Guifang Zhao [b], Zhen Shi [a]

[a] Ministry of Education Key Laboratory of Synthetic and Natural Functional Molecule Chemistry, College of Chemistry & Materials Science, Northwest University, Xi'an, Shaanxi 710069, PR China
[b] College of Life Sciences, Northwest University, Xi'an, Shaanxi 710069, PR China
[c] College of Chemistry, Beijing Normal University, Beijing 100875, PR China

ARTICLE INFO

Article history:
Received 14 August 2011
Received in revised form
17 September 2011
Accepted 20 September 2011
Available online 29 September 2011

Keywords:
Rhodamine
Fluorescent chemosensor
Theoretical computation
Mechanism
Fe^{3+}
X-ray crystallography

ABSTRACT

A novel rhodamine based probe has been synthesized as an "off–on" chemosensor for Fe^{3+}. Upon coordination with Fe^{3+}, the probe displayed good brightness and fluorescent enhancement. A linear relationship was observed to exist between the relative fluorescence intensity of this probe and the concentration of Fe^{3+} in the range of 5 μM–20 μM with a detection limit of 5 μM. It offered highly sensitive toward Fe^{3+} over other ions. The recognizing behaviors toward Fe^{3+} have been investigated both experimentally and computationally. It can be expected that Fe^{3+} coordinated with the N atom of thiazole moiety in the probe accompanied by the transferring of electrons of the phenylthiazole resulted in the opening of the spiro-ring.

1. Introduction

The development of artificial chemosensors for selective and sensitive quantification of environmentally and biologically important ionic species in solution, especially for heavy and transition metal ions, has attracted a great deal of attention [1–3]. As one of the most essential trace elements in biological systems, Fe^{3+} performs a major role in the growth and development of living systems as well as in many biochemical processes at the cellular level [4,5]. Numerous enzymes use Fe^{3+} as a catalyst for oxygen metabolism, detective transfer as well as DNA and RNA synthesis [6,7]. High levels of Fe^{3+} within the body have been associated with increasing incidence of certain cancers and dysfunction of certain organs, such as heart, pancreas and liver [8–11]. Some recent research results suggested that Fe^{3+} could also be involved in the underlying mechanisms of many neurodegenerative diseases, such as Parkinson's disease and Alzheimer's disease [12–14]. The essential role of iron in human and animal health became apparent during this past century with identification of Fe^{3+} as a body constituent and realization of the relationship between adequate Fe^{3+} intake and prevention of certain diseases [15–18].

Although significant contributions to the development of spectroscopic sensing for Fe^{3+} have been made over the last few decades, there have been relatively few fluorescent chemosensors for Fe^{3+} due to the fluorescent quenching of the paramagnetic Fe^{3+} [19–22]. Recently, Lee et al. [23] have developed a Fe^{3+}-selective chemosensor FS1 which could demonstrate sensitive and selective detection of intracellular Fe^{3+} in hepatocytes. Another rhodamine 6G derivative reported by Wang et al. [24] could detect Fe^{3+} among various metal ions in water with the detection limit reaching as low as 2 ppb. At present, there is an intense demand for new efficient Fe^{3+} chemosensors. Works related to this area are of great challenge and interest.

On the other hand, as a simple, efficient and economic method, fluorescent signaling has been widely used in biological and environmental science [25–28]. Owing to their simplicity, low detection limit, the capability for special recognition and excellent spectroscopic properties, such as long wavelength excitation and emission profiles, large extinction coefficient and high fluorescence quantum yields [29,30], rhodamine dyes appear to be particularly

* Corresponding author. Tel.: +8629 88302604; fax: +8629 88302601.
E-mail address: lijianli@nwu.edu.cn (J. Li).

0143-7208/$ – see front matter © 2011 Elsevier Ltd. All rights reserved.
doi:10.1016/j.dyepig.2011.09.014

attractive for the construction of an OFF–ON-type fluorescent chemosensor. Recently, on the basis of spirolactam (non-fluorescent) to ring-open amide (fluorescent) equilibrium of rhodamine, a number of rhodamine derivatives have been utilized for the detection of metal ions, such as Cu^{2+}, Hg^{2+}, Cr^{3+}, Pb^{2+}, Au^{+} [31–35]. With these criteria in mind, herein we introduced a phenylthiazole moiety to rhodamine B and obtained a new fluorescent probe **S1** (Scheme 1, synthesis), which can give a highly selective and rapid spectroscopic response to Fe^{3+}.

2. Experimental

2.1. Apparatus and reagents

The fluorescence spectra measurements were performed on a HITACHI F-4500 fluorescence spectrophotometer. Absorbance spectra measurements were carried out on a Shimadzu UV-1700 spectrophotometer. Mass spectra were measured with Model AXIMA-CFR™ plus MALDI-TOF Mass Spectroscopy. IR spectra were taken in KBr disks on a Bruker Tensor 27 spectrometer. X-ray crystal data were collected on Bruker Smart APEX II CCD diffractometer. NMR spectra were recorded on a Varian INOVA-400 MHz spectrometer (at 400 MHz for ^{1}H NMR and 100 MHz for ^{13}C NMR) with tetramethylsilane (TMS) as internal standard. Rhodamine B, acetophenone, iodine, thiourea, anhydrous $FeCl_3$ and methanol were all obtained from J&K Scientific Ltd. The solutions of metal ions were performed from their nitrate and chloride salts. Analytical thin layer chromatography was performed using Merck 60 GF254 silica gel (precoated sheets, 0.25 mm thick). Silica gel (0.200–0.500 mm, 60A, J&K Scientific Ltd.) was used for column chromatography. All the reagents were of analytical-reagent grade. Double distilled water was used throughout the experiment.

2.2. Synthesis routes

2.2.1. Synthesis of 2-amino-4-phenylthiazole

12.0 g (0.1 mol) of acetophenone, 25.4 g (0.1 mol) of iodine and 15.2 g (0.2 mol) of thiourea were well crushed in crucible. The mixture was taken in 250 mL round bottom flask and heated at 110 °C for 24 h. A reaction mixture was cooled to room temperature and diluted with 100 mL of water and extracted with ether to remove the unreacted iodine and acetophenone. Excess of ether was distilled off. Residue was dissolved in boiling water and filtered off the hot solution. It was allowed to stand for 30 min. Make the reaction mixture alkaline (up to pH 8–9) using ammonium hydroxide solution. The solid obtained was filtered and washed successively with water (2 × 150 mL). The separated solid was crystallized by aqueous ethanol (1:1) to give 12.0 g solid, yield: 68%. mp: 147–148 °C (Reported [36] mp: 147 °C). Anal. Calcd for $C_9H_8N_2S$: H, 4.58; C, 61.34; N, 15.90; S, 18.19. Found: H, 4.60; C, 61.40; N, 15.86; S, 18.14. ^{1}H NMR (400 MHz, $CDCl_3$, TMS): δ 7.80 (d, J = 8.0 Hz, 2H), 7.41 (t, J = 8.0 Hz, 2H), 7.32 (t, J = 8.0 Hz, 1H), 6.76 (s, 1H), 5.12 (s, 2H).

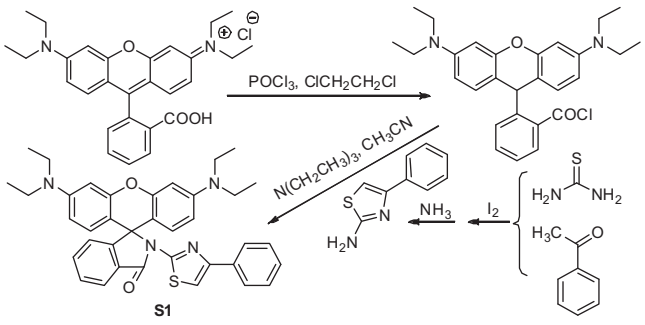

Scheme 1. Synthesis of rhodamine based probe **S1**.

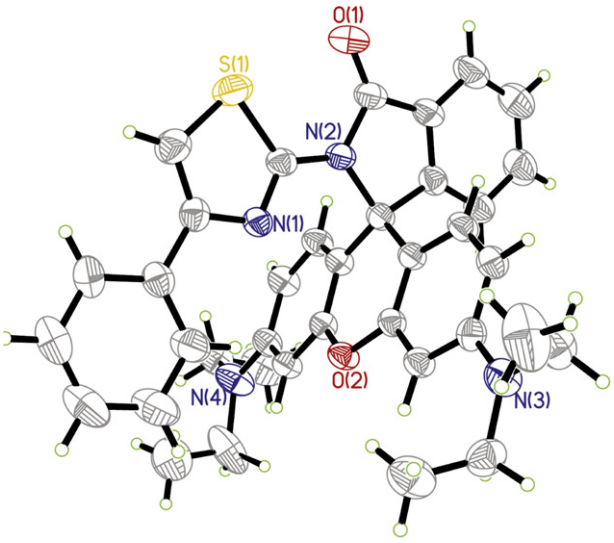

Fig. 1. Molecular structure of probe **S1**.

2.2.2. Synthesis of probe *S1*

In brief, to a stirred solution of rhodamine hydrochloride (4.78 g, 0.01 mol) in 1,2-dichloroethane (10 mL), 5 mL phosphorus oxychloride was added. The solution was refluxed for 6 h and concentrated by evaporation. The obtained crude acid chloride was dissolved in acetonitrile (10 mL), a solution of 2-amino-4-phenylthiazole (1.76 g, 0.01 mol), triethylamine (5 mL) in acetonitrile (20 mL) was added dropwise in 30 min. After refluxing for 4 h, the solvent was removed under reduce pressure to give violet oil. Water was then added to the mixture and the aqueous was extracted with dichloromethane (15 mL × 3). The organic layer was washed with water and dried over anhydrous $MgSO_4$ and filtered.

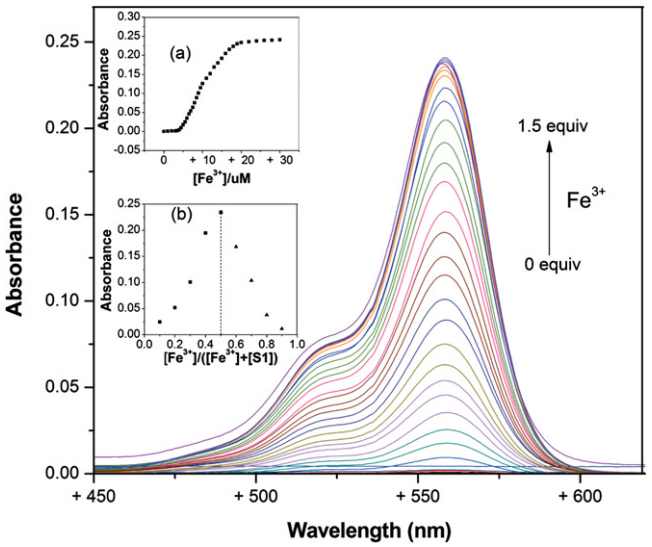

Fig. 2. Changes in UV–Vis absorption spectra of **S1** (20 μM) in methanol solution with various amounts of Fe^{3+} (0–1.5 equiv). Inset: (a). Absorbance at 558 nm of **S1** as a function of Fe^{3+} concentration; (b). Job's plot of **S1** and Fe^{3+}. The total concentration of **S1** and Fe^{3+} was 100 μM. The absorbance was measured at 558 nm.

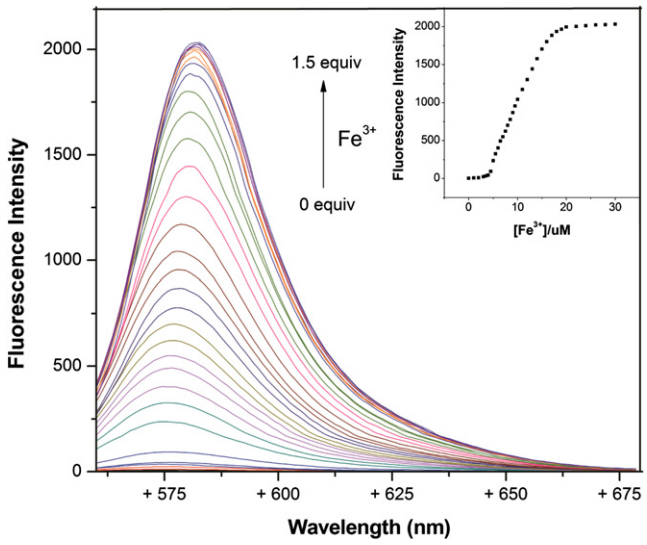

Fig. 3. Fluorescence spectra changes of **S1** (20 μM) in methanol solution upon addition of Fe^{3+} (0–1.5 equiv), λ_{ex} = 558 nm. Inset: Changes in the emission intensity at 580 nm.

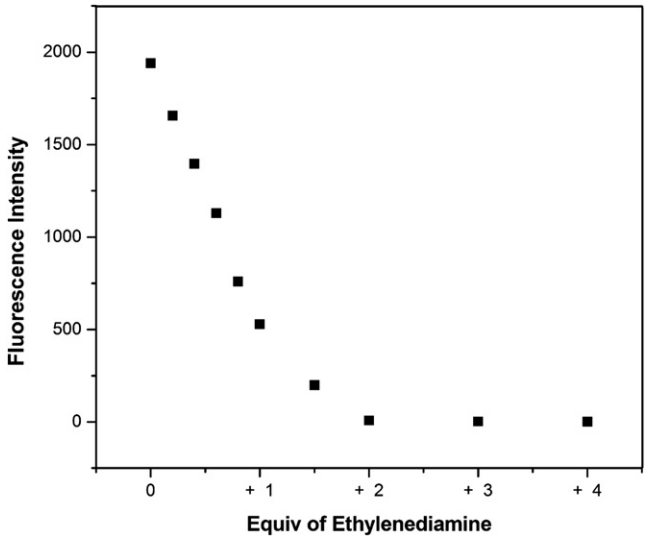

Fig. 4. Fluorescence intensity changes of **S1** (20 μM) upon the addition of each equiv of ethylenediamine with the presence of Fe^{3+} (20 μM) in methanol solution.

The product was purified by column chromatography on silica gel (eluent: CH_2Cl_2) to give 3.12 g yellow powder, yield: 52%. mp: 269–270 °C. Anal. Calcd for $C_{37}H_{36}N_4O_2S$: H, 6.04; C, 73.97; N, 9.33; S, 5.34. Found: H, 6.03; C, 73.77; N, 9.35; S, 5.35. ^{1}H NMR (400 MHz, $CDCl_3$, TMS): δ 8.072 (d, J = 7.2 Hz, 1H), 7.865 (d, J = 6.8 Hz, 2H), 7.590 (q, J = 8 Hz, 2H), 7.374 (t, J = 6.8 Hz, 2H), 7.284–7.250 (m, 2H), 7.046 (s, 1H), 6.474 (d, J = 3.6 Hz, 2H), 6.410 (d, J = 8.8 Hz, 2H), 6.164 (d, J = 8.8 Hz, 2H), 3.286 (q, J = 8.4 Hz, 8H), 1.112 (t, J = 7.2 Hz, 12H). ^{13}C NMR (100 MHz, $CDCl_3$, TMS): δ 12.59, 44.30, 67.74, 76.74, 77.06, 77.36, 97.45, 106.34, 106.73, 107.16, 123.31, 124.87, 126.09, 127.29, 128.19, 128.23, 128.64, 129.52, 134.16, 134.84, 148.73, 150.10, 153.36, 154.25, 154.28, 166.39.

2.3. Crystal growth and conditions

Yellow single crystal of **S1** was obtained at room temperature from the mixed solvents of acetonitrile-dichloromethane-dioxane (5:3:2, v/v/v) solution by slow evaporation, and then mounted on the goniometer of single crystal diffractometer. The crystal data has been collected at 296 K by using Mo $K\alpha$ radiation (λ = 0.71073 Å) the θ range of 1.78–25.10° by using φ/ω scan mode and collected for Lorentz and polarization effect (SADABS). The structure was solved using the direct method and refined by full-matrix least-squares fitting on F^2 by SHELX-97. Crystal data for **S1**: Crystal size: 0.33 × 0.27 × 0.15 mm, monoclinic, space group $P2_1/n$. a = 12.0495(17), b = 18.109(3), c = 14.957(2), $\alpha = \gamma = 90°$, β = 99.638(2)°, V = 3217.6(8) Å^3, Z = 4, 15,989 reflections collected, 5718 unique (R_{int} = 0.0494). Final residual for 402 parameters and 5718 reflections with $I > 2\sigma(I)$: R_1 = 0.0584, wR_2 = 0.1516 and GOF = 1.27.

2.4. UV–vis and fluorescence spectra measurements

2.4.1. *S1* stock solution

S1 stock solution (500 μM): in a 25 mL volumetric flask, 0.0939 g **S1** probe was dissolved in acetone and then diluted to the mark with acetone. To a 50 mL volumetric tube, 4.00 mL of the solution was added and diluted to 50 mL with methanol.

2.4.2. Fe^{3+} stock solution

Fe^{3+} stock solution (5.00 mM): in a 25 mL volumetric flask, 20.27 mg anhydrous $FeCl_3$ was dissolved in methanol and then diluted to the mark with methanol. The other metal ions were prepared as 5.00 mM in methanol solution.

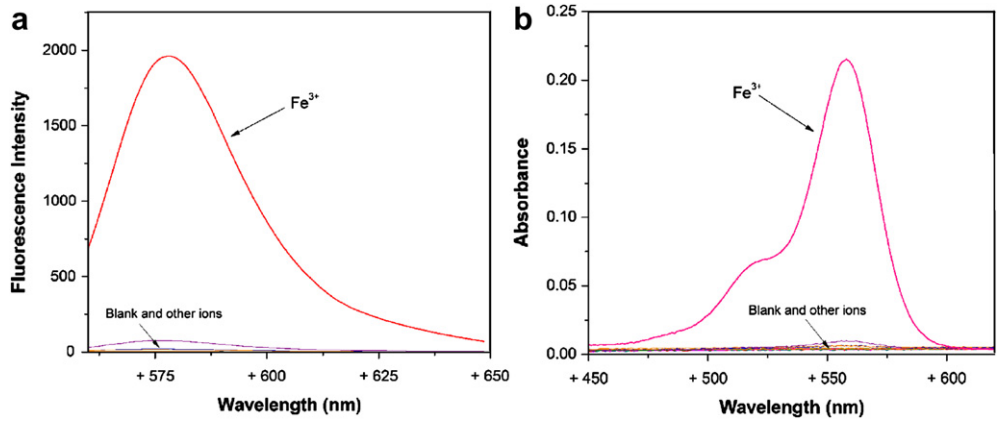

Fig. 5. Fluorescence (a) and absorption (b) spectra of **S1** (20 μM) in methanol solution upon addition of various metal ions (20 μM), λ_{ex} = 558 nm.

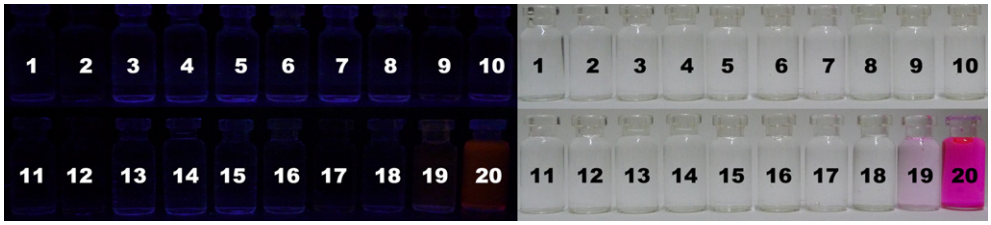

Fig. 6. Fluorescent and color changes of **S1** (20 μM) upon the addition various metal ions (20 μM). 1: blank; 2: Li^+; 3: Na^+; 4: K^+; 5: Ba^{2+}; 6: Ca^{2+}; 7: Cd^{2+}; 8: Ag^+; 9: Mg^{2+}; 10: Co^{2+}; 11: Mn^{2+}; 12: Zn^{2+}; 13: Pb^{2+}; 14: Hg^{2+}; 15: Ni^{2+}; 16: Cu^+; 17: Cu^{2+}; 18: Fe^{2+}; 19: Fe^{3+}.

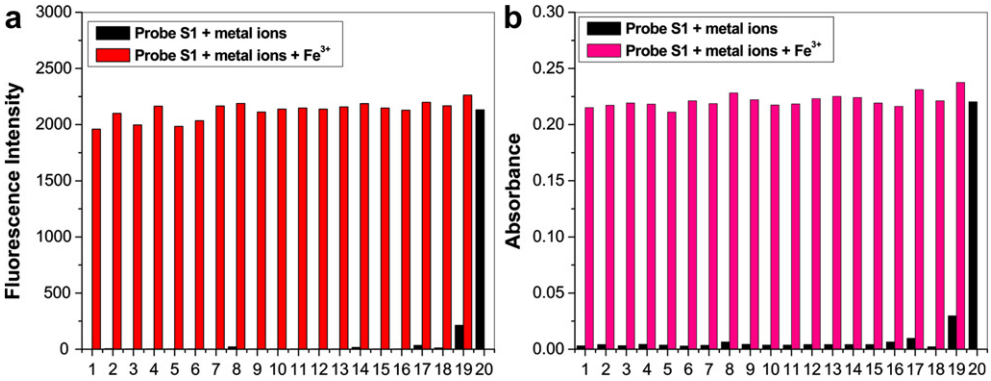

Fig. 7. Fluorescence intensity (a) and absorption (b) changes of **S1** (20 μM) upon the addition of various metal ions (20 μM) in and without the presence of Fe^{3+} (20 μM) in methanol solution. Black bars represent the fluorescence response of **S1** to the metal ions of interest. 1: blank; 2: Li^+; 3: Na^+; 4: K^+; 5: Ba^{2+}; 6: Ca^{2+}; 7: Cd^{2+}; 8: Ag^+; 9: Mg^{2+}; 10: Co^{2+}; 11: Mn^{2+}; 12: Zn^{2+}; 13: Pb^{2+}; 14: Hg^{2+}; 15: Ni^{2+}; 16: Cu^+; 17: Cu^{2+}; 18: Fe^{2+}; 19: Fe^{3+}. The chromatic bars represent the subsequent addition of 20 μM Fe^{3+} to the above solutions.

2.4.3. Procedure for colorimetric method

For colorimetric determination of Fe^{3+}, 1.00 mL of 500 μM **S1** stock solution and different concentration of Fe^{3+} to a 25 mL volumetric tube, and then diluted to the mark with methanol, then the absorbance was recorded at 558 nm.

2.4.4. Procedure for fluorimetric method

To a 25 mL volumetric tube, 1.00 mL of 500 μM **S1** stock solution, different concentration of Fe^{3+} were added and the mixture was diluted to 25 mL with methanol. Then, 3.0 mL each solution was transferred to a 1 cm cuvette and the fluorescence intensity of the above solution was recorded at 580 nm with excitation wavelength set at 558 nm. The excitation and emission wavelength bandpasses were both set at 5.0 nm.

2.5. Computation details

Density functional theory (DFT) [37] calculations were performed at B3LYP [38,39] level with Guassian 03 [40] Program. Fe element was described with TZVP basis set [41], Cl element was described with 6-311++G** basis set [42], S, N and O elements were described with 6-31++G* basis set [42] and 6-31G** [42] basis set was used for C and H elements. Default type of grids in Guassian 03 Program for the numerical integration in DFT calculations was utilized.

3. Results and discussion

3.1. Synthesis and structure characterization

As shown in Scheme 1, **S1** was facilely synthesized from rhodamine B by an uncomplicated reaction with a yield of 52%. The structure was confirmed by IR, ^1H NMR, ^{13}C NMR spectra and X-ray crystallography (the spectra are shown in Supporting information).

The ORTEP structure of **S1** was shown in Fig. 1. The single crystal structure of **S1** clearly revealed the unique spirolactam ring formation. In this probe, the bond lengths are in the normal range, such as N2–C9 (1.3844 Å), N2–C17 (1.512 Å), N2–C10 (1.3844 Å), C17–C29 (1.5034 Å), C17–C18 (1.5204 Å), C26–N4 (1.3724 Å) and C21–N3 (1.3874 Å) et al. In addition, the dihedral angle between the thiazole ring and xanthene ring plane is 89.67°. There also exist two kinds of hydrogen bonding interaction in the complex, that is,

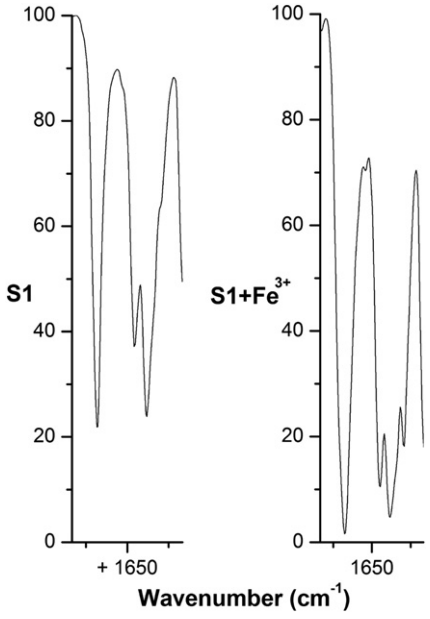

Fig. 8. IR of **S1** and **S1** + $FeCl_3$.

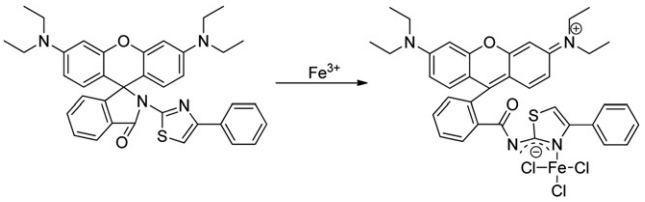

Scheme 2. Proposed mechanism for the fluorescent changes of **S1** upon the addition of Fe^{3+}.

C5–H5···O2 (H5···O2, 2.713 Å) and C19–H19···O1 (H19···O1, 2.614 Å), which can help the molecule extend and stabilize the three dimensional supramolecular structure.

3.2. Spectral characteristics

Absorption spectra of **S1** were performed in methanol solution (Fig. 2). The free probe of **S1** was colorless and scarcely showed absorption at 558 nm. Upon binding with Fe^{3+}, the absorption peak intensity increased dramatically, coupled with a clear color change from colorless to pink. This implied that **S1** allowed naked-eye detection for Fe^{3+}. Absorption titrations showed a typical sigmoidal curve and the increase was saturated with more than 1.0 equiv of Fe^{3+} (Fig. 2(a), inset). Job's plot for the absorbance was applied to study the binding mode of **S1** and Fe^{3+}. The association constant was estimated [43,44] to be 6.56×10^4 M^{-1} from the absorption titrations experiments based on the basis of nonlinear fitting of the titration curve assuming the 1:1 binding model (Fig. 2(b), inset).

Fig. 3 shows the results of fluorescence titration of **S1** upon the gradual addition of Fe^{3+} in methanol solution under excitation at $\lambda = 558$ nm. No obvious fluorescent emission was observed around 580 nm in the absence of iron because the spirocyclic form of rhodamine prevailed. Upon the addition of increasing concentration of the Fe^{3+}, the intensity increased drastically which was reasonably assigned to the delocalized xanthene tautomer of the rhodamine group indicating the ring-opened process of rhodamine B unit in **S1**. The increment saturated after adding 1.0 equiv of Fe^{3+} (Fig. 3, inset). The fluorescence quantum yield was calculated [45] as 0.34 by using rhodamine B as a standard. A linear relationship was observed to exist between the relative fluorescent intensity of **S1** and the concentration of Fe^{3+} in the range of 5 μM–20 μM with a detection limit of 5 μM. Addition of ethylenediamine to the mixture of **S1** (20 μM) and Fe^{3+} (20 μM) decreased the fluorescence intensity of the solution (Fig. 4) and the color of the mixture changed back to colorless, which implied the reversible binding between **S1** and Fe^{3+}.

For an excellent chemosensor, high selectivity is a matter of necessity. Related metal ions, including Li^+, Na^+, K^+, Ba^{2+}, Ca^{2+}, Cd^{2+}, Mg^{2+}, Co^{2+}, Mn^{2+}, Zn^{2+}, Pb^{2+}, Ni^{2+}, Hg^{2+}, Ag^+, Cu^+, Cu^{2+}, $Fe^{2+}$and Cr^{3+}, were used to evaluate the metal ion binding properties of **S1** in methanol solution by fluorescence spectroscopy and UV–Vis spectroscopy. Among the various metal ions, both the absorption and the fluorescence emission spectra showed a noteworthy high selectivity to Fe^{3+} with respect to the large color changes and fluorescent enhancement. Other metal ions developed no significant absorption and fluorescence intensity changes (Figs. 5 and 6). The competition experiment, which was carried out by adding Fe^{3+} to **S1** solution in the presence of other metal ions, showed that the Fe^{3+}-induced fluorescent response was not interfered by the commonly coexistent ions. The result suggested that probe **S1** showed a remarkable selectivity toward Fe^{3+} over other competitive ions (Fig. 7).

3.3. Theoretical computation and mechanism

In the IR spectra (Fig. 8), the peak at 1703 cm^{-1}, corresponding to the characteristic carbonyl absorption of **S1**, did not drastically shift to the lower frequency upon addition of 1.0 equiv of $FeCl_3$, This supported that the amide carbonyl oxygen was actually not involved in the coordination.

In order to obtain a deep understanding of the new probe **S1**, DFT calculations of **S1** and **S1**–Fe^{3+} complex were performed. Fig. 8 showed the optimized geometries of **S1** and **S1**–Fe^{3+} complex, of which the local minimum character was confirmed by the nonexistence of imaginary frequency [42]. The bond length of N4–C26 changed from 1.387 Å (**S1**) to 1.359 Å (**S1**–Fe^{3+}), while the length of C17–C29 changed from 1.516 Å (**S1**) to 1.409 Å (**S1**–Fe^{3+}), indicating the existence of the quinoid structure in **S1**–Fe^{3+} (Fig. 8). This fact suggested the ring-opening progress in **S1** upon coordination with Fe^{3+}. In the case of previous works, coordination of carbonyl oxygen to metal ions leaded to spirocycle opening [46,47]. While this study, it was clear shown that, in the lowest energy structure of the **S1**–Fe^{3+} complex, Fe^{3+} ion was mainly coordinated with the N on the phenylthiazole moiety of **S1** with the average distance of 1.925 Å which was much shorter than the sum of the Van der Waals radii of Fe and N (3.35 Å). On the other hand, the distance between O atom and Fe was 5.300 Å, longer than the sum of the Van der Waals radii (3.34 Å), indicating that O atom was hard to coordinate with Fe^{3+}. It is probable that the positive charge of the Fe^{3+} was significantly decreased by coordination with the thiazole nitrogen which made Fe^{3+} hard to coordinate with carbonyl

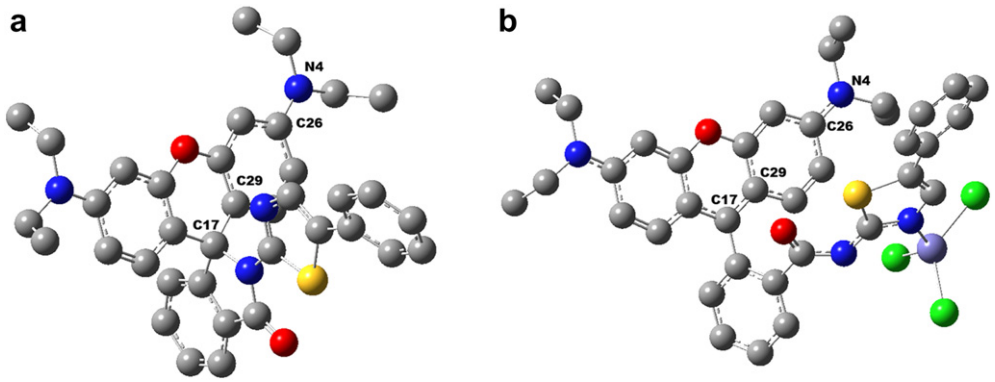

Fig. 9. B3LYP optimized structure of **S1**(a) and **S1**–Fe^{3+}(b) complex. Carbon atoms are gray, oxygen atoms are red, nitrogen atoms are blue, sulfur atoms are yellow, chlorine atoms are green, and iron atom is steelblue. (For interpretation of the references to color in this figure legend, the reader is referred to the web version of this article.)

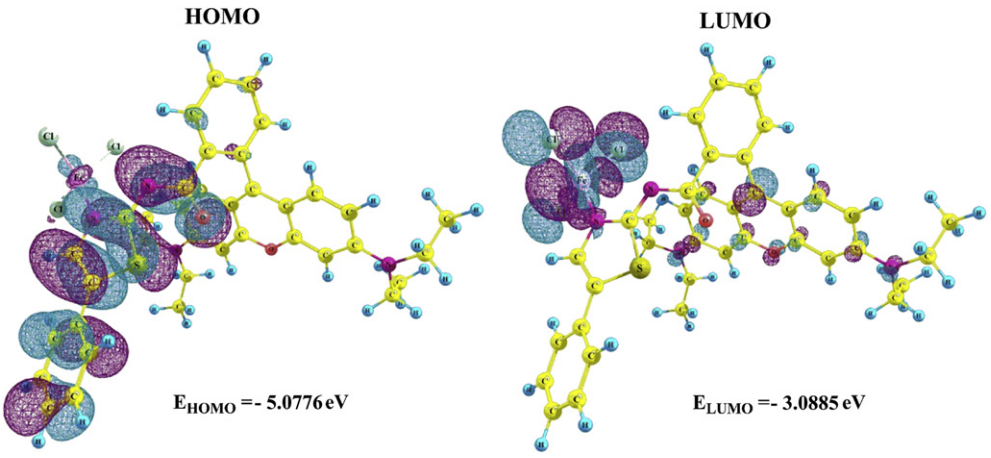

Fig. 10. HOMO and LUMO distributions of **S1**–Fe^{3+}.

oxygen. All in all, it can be expected that Fe^{3+} coordinated with the N atom of thiazole moiety in **S1** accompanied by the transferring of electrons of the phenylthiazole resulted in the opening of the spiro-ring (Scheme 2).

The spatial distributions and orbital energies of HOMO and LUMO of **S1**–Fe^{3+} were also determined (Fig. 9). It was clearly shown that the HOMO distribution of the complex was located essentially over the phenylthiazole moiety, while the LUMO was mainly distributed over Fe^{3+} and neighboring atoms. The energy gap between HOMO and LUMO was computed to be 1.985 eV (Fig. 10).

4. Conclusion

In conclusion, a novel rhodamine based "off–on" fluorescent chemosensor bearing a phenylthiazole moiety has been synthesized for the selective and sensitive detection of Fe^{3+}. The sensor showed a remarkable enhancement of the fluorescence intensity and a clear color change from colorless to pink upon binding with Fe^{3+}. The response of the sensor to Fe^{3+} was unaffected by the presence of other common coexistent metal ions. Theoretical studies supported that the Fe^{3+} binding to N atom of thiazole moiety in **S1** accompanied by the transferring of electrons of the phenylthiazole drove the structural changes.

Acknowledgments

The project was supported by National Natural Science Foundation of China (No. 20972124), the China Postdoctoral Science Foundation (No. 20080441180), the Chinese National Science Foundation for Talent Training (No. J0830417) and the Chinese National Innovation Experiment Program for University Students (No. 20101069702). Y.B. wants to express his thanks to Prof. Yuanhe Huang (College of Chemistry, Beijing Normal University) for his great help.

Appendix. Supplementary data

Supplementary material associated with this article can be found, in the online version, at doi:10.1016/j.dyepig.2011.09.014, http://www.sciencedirect.com.

References

[1] De Silva AP, Gunaratne HQ, Gunnlaugsson T, Huxley AJ, McCoy CP, Rademacher JT, et al. Signaling recognition events with fluorescent sensors and switches. Chem Rev 1997;97:1515–66.
[2] Martinez-Manez R, Sancenon F. Fluorogenic and chromogenic chemosensors and reagents for anions. Chem Rev 2003;103:4419–76.
[3] Kim HN, Lee MH, Kim HJ, Kim JS, Yoon J. A new trend in rhodamine-based chemosensors: application of spirolactam ring-opening to sensing ions. Chem Soc Rev 2008;37:1465–72.
[4] D'Autreáux B, Tucker NP, Dixon R, Spiro SA. Non-haem iron centre in the transcription factor NorR senses nitric oxide. Nature 2005;437:769–72.
[5] Lee JW, Helmann JD. The PerR transcription factor senses H_2O_2 by metal-catalysed histidine oxidation. Nature 2006;440:363–7.
[6] Weizman H, Ardon O, Mester B, Libman J, Dwir O, Hadar Y, et al. Fluorescently-labeled ferrichrome analogs as probes for receptor-mediated, microbial iron uptake. J Am Chem Soc 1996;118:12368–75.
[7] Sumner JP, Kopelman R. Alexa Fluor 488 as an iron sensing molecule and its application in PEBBLE nanosensors. Analyst 2005;130:528–33.
[8] Halliwell B. Reactive oxygen species and central nervous system. J Neurochem 1992;59:1609–23.
[9] Weinberg ED. The role of iron in cancer. Eur J Cancer Prev 1996;5:19–36.
[10] Swaminathan S, Fonseca VA, Alam MG, Shah SV. The role of iron in diabetes and its complications. Diabetes Care 2007;30:1926–33.
[11] Galaris D, Skiada V, Barbouti A. Redox signaling and cancer: the role of "labile" iron. Cancer Lett 2008;266:21–9.
[12] Kaur D, Rajagopalan S, Andersen JK. Chronic expression of H-ferritin in dopaminergic midbrain neurons results in an age-related expansion of the labile iron pool and subsequent neurodegeneration: implications for Parkinson's disease. Brain Res 2009;1297:17–22.
[13] Kozlowski H, Janicka-Klos A, Brasun J, Gaggelli E, Valensin D, Valensin G. Copper, iron, and zinc ions homeostasis and their role in neurodegenerative disorders (metal uptake, transport, distribution and regulation). Coord Chem Rev 2009;253:2665–85.
[14] Schneider SA, Bhatia KP. Three faces of the same gene: FA2H links neurodegeneration with brain iron accumulation, leukodystrophies, and hereditary spastic paraplegias. Ann Neurol 2010;68:575–7.
[15] Neilands JB. A brief history of iron metabolism. Biol Met 1991;4:1–6.
[16] Ajioka RS, Kushner JP. Clinical consequences of iron overload in hemochromatosis homozygotes. Comments Blood 2003;101:3351–4.
[17] Zimmermann MB, Hurrell RF. Nutritional iron deficiency. Lancet 2007;370:511–20.
[18] Collins JF, Prohaska JR, Knutson MD. Metabolic crossroads of iron and copper. Nutr Rev 2010;68:133–47.
[19] Bricks JL, Kovalchuk A, Trieflinger C, Nofz M, Bueschel M, Tolmachev I, et al. On the development of sensor molecules that display Fe^{III}-amplified fluorescence. J Am Chem Soc 2005;127:13522–9.
[20] Xiang Y, Tong AJ. A new rhodamine-based chemosensor exhibiting selective Fe^{III}-amplified fluorescence. Org Lett 2006;8:1549–52.
[21] Zhang X, Shiraishi Y, Hirai T. A new rhodamine-based fluorescent chemosensor for transition metal cations synthesized by one-step facile condensation. Tetrahedron Lett 2007;48:5455–9.
[22] Dong L, Wu C, Zeng X, Mu L, Xue SF, Tao Z, et al. The synthesis of a rhodamine B Schiff-base chemosensor and recognition properties for Fe^{3+} in neutral ethanol aqueous solution. Sens Actuators B: Chem 2010;145:433–7.
[23] Lee MH, Giap TV, Kim SH, Lee YH, Kang C, Kim JS. A novel strategy to selectively detect Fe(III) in aqueous media driven by hydrolysis of a rhodamine 6G Schiff base. Chem Commun 2010;46:1407–9.
[24] Wang BD, Hai J, Liu ZC, Wang Q, Yang ZY, Sun SH. Selective detection of iron(III) by rhodamine-modified Fe_3O_4 nanoparticles. Angew Chem Int Ed 2010;49:4576–9.
[25] Malashikhin S, Finney NS. Fluorescent signaling based on sulfoxide pro-fluorophores: application to the visual detection of the explosive TATP. J Am Chem Soc 2008;130:12846–7.

[26] Ostergaard ME, Cheguru P, Papasani MR, Hill RA, Hrdlicka PJ. Glowing locked nucleic acids: brightly fluorescent probes for detection of nucleic acids in cells. J Am Chem Soc 2010;132:14221–8.
[27] Guo ZQ, Zhu WH, Zhu MM, Wu XM, Tian H. Near-Infrared Cell-Permeable Hg^{2+}-selective ratiometric fluorescent chemodosimeters and fast indicator paper for $MeHg^{+}$ based on tricarbocyanines. Chem Eur J 2010;16:14424–32.
[28] Tan SS, Kim SJ, Kool ET. Differentiating between fluorescence-quenching metal ions with polyfluorophore sensors built on a DNA backbone. J Am Chem Soc 2011;133:2664–71.
[29] Zou Q, Jin JY, Xu B, Ding L, Tian H. New photochromic chemosensors for Hg^{2+} and F^{-}. Tetrahedron 2011;67:915–21.
[30] Ramette RW, Sandell EB. Rhodamine B equilibriums. J Am Chem Soc 1956;78: 4872–8.
[31] Royzen M, Dai ZH, Canary JW. Ratiometric displacement approach to Cu(II) sensing by fluorescence. J Am Chem Soc 2005;127:1612–3.
[32] Zhang XL, Xiao Y, Qian XH. A ratiometric fluorescent probe based on FRET for imaging Hg^{2+} ions in living cells. Angew Chem Int Ed 2008;47:8025–9.
[33] Huang KW, Yang H, Zhou ZG, Yu MX, Li FY, Gao X, et al. Multisignal chemosensor for Cr^{3+} and its application in bioimaging. Org Lett 2008;10:2557–60.
[34] Kwon JY, Jang YJ, Lee YJ, Kim KM, Seo MS, Nam W, et al. A highly selective fluorescent chemosensor for Pb^{2+}. J Am Chem Soc 2005;127:10107–11.
[35] Yang Y, Lee S, Tae J. A gold(III) ion-selective fluorescent probe and its application to bioimagings. Org Lett 2009;11:5610–3.
[36] Dodson RM, King LC. Reaction of ketones with halogens and thiourea. J Am Chem Soc 1945;67:2242–3.
[37] Koch W, Holthausen MC. A chemist's guide to density functional theory. New York: Wiley; 2000.
[38] Becke AD. Density-functional thermochemistry. III. The role of exact exchange. J Chem Phys 1993;98:5648–52.
[39] Lee C, Yang W, Parr RG. Development of the Colle-Salvetti correlation-energy formula into a functional of the electron density. Phys Rev B 1988; 37:785–9.
[40] Frisch MJ, Trucks GW, Schlegel HB, Scuseria GE, Robb MA, Cheeseman JR, et al. Gaussian 03. Pittsburgh PA: Gaussian Inc; 2003.
[41] Schäfer A, Huber C, Ahlrichs R. Fully optimized contracted Gaussian basis sets of triple zeta valence quality for atoms Li to Kr. J Chem Phys 1994;100: 5829–35.
[42] Foresman JB, Frisch AE. Exploring chemistry with electronic structure methods. 2th ed. Pittsburgh PA: Gaussian Inc; 1996.
[43] Bourson J, Pouget J, Valeur B. Ion-responsive fluorescent compounds. 4. Effect of cation binding on the photophysical properties of a coumarin linked to monoaza- and diaza-crown ethers. J Phys Chem 1993;97:4552–7.
[44] Zhao Y, Zhang XB, Han ZX, Qiao L, Li CY, Jian LX, et al. Highly sensitive and selective colorimetric and off–on fluorescent chemosensor for Cu^{2+} in aqueous solution and living cells. Anal Chem 2009;81:7022–30.
[45] Huang W, Song CX, He C, Lv GJ, Hu XY, Zhu X, et al. Recognition preference of rhodamine-thiospirolactams for mercury(II) in aqueous solution. Inorg Chem 2009;48:5061–72.
[46] Wu DY, Huang W, Duan CY, Lin ZH, Meng QJ. Highly sensitive fluorescent probe for selective detection of Hg^{2+} in DMF aqueous media. Inorg Chem 2007;46:1538–40.
[47] Huang W, Zhu X, Wua DY, He C, Hu XY, Duan CY. Structural modification of rhodamine-based sensors toward highly selective mercury detection in mixed organic/aqueous media. Dalton Trans; 2009:10457–65.